Available online at www.sciencedirect.com
ScienceDirect
Journal of Power Sources 165 (2007) 625–629
JOURNAL OF POWER SOURCES
www.elsevier.com/locate/jpowsour

Short communication

Aluminum substituted manganese oxides for lithium battery applications

E. Machefaux, A. Verbaere, D. Guyomard *

Laboratoire de Chimie des Solides, Institut des Matériaux Jean Rouxel, CNRS, Université de Nantes, B.P. 32229, 44322 Nantes Cedex 3, France

Available online 15 November 2006

Abstract

Using the electrochemical–hydrothermal method, Al-substituted MnO_2 materials with α- or γ-structures or mixtures of these phases have been synthesized. The Al-substituted materials are highly disordered and are characterized by a large amount of microtwinning defects compared to non substituted ones synthesized under the same conditions. The effect of the presence of aluminum on the physico-chemical, structural and morphological properties are presented. The presence of Al^{III} allows obtaining "interconnected nanowires" of $Mn_{1-y}Al_yO_{2-\delta}$ with very high surface areas. The lithium insertion properties of the Al-substituted γ-MnO_2 materials are discussed by comparison to non substituted ones.

Keywords: Manganese dioxides; Aluminum substitution; Nanowires; Li batteries

1. Introduction

MnO_2-based oxides are very attractive as active materials in the positive electrode for Li-metal primary and secondary batteries due to their economical advantages and their low toxicity. The Hollandite α-MnO_2 structure has been widely investigated, over the past years, as positive electrode material in lithium rechargeable batteries. From a fundamental point of view, the γ-MnO_2 family is particularly attractive due to its completely flexible network offering infinity of structural possibilities. As a matter of fact, the structure of these materials is composed of a random intergrowth of ramsdellite (double chains of MnO_6 octahedra arranged so as to delimit channels with the size of 2 edges of octahedron by 1 edge of octahedron, noted 2×1 channels) and pyrolusite (β-MnO_2, single chains of MnO_6 octahedra, 1×1 channels) structures [1], in which reversible lithium insertion is possible. The γ-MnO_2 structure also contains microtwinning defects [2], which basically correspond to changes in the direction of the channels (i.e. of the *c*-axis) by 60° or 120°. The relative concentrations of pyrolusite (P_r, in percent) and microtwinning (Mt, in percent) defects can be estimated from simulation of the powder X-ray diffraction patterns [2,3]. The γ-MnO_2 compounds are thus structurally characterized by the couple of structural parameters (P_r, Mt). For extensively twinned samples, Chabre and Pannetier [2] have shown that the diffraction pattern contains only few broad lines, because the (h21) and (h40) lines have merged. In this case, the amount of microtwinning defects Mt can be estimated as superior or equal to 50%, but cannot be determined more precisely.

In previous study [4], our group has chosen to explore the electrochemical–hydrothermal method for the synthesis of MnO_2 materials approaching the ramsdellite limit. Although the first results were promising [4], γ-MnO_2 materials synthesized by this route deliver too low a cycled capacity. To try to modify the electrode behavior of γ-MnO_2 compounds, we have chosen to substitute the manganese in these materials with aluminum. The choice of aluminum as a substituting element has been done on the basis of some suggestion from the literature [5] and by considering the radius of Al^{III}, which is close to that of Mn^{IV}.

We report here the synthesis of Al-substituted manganese dioxides by the electrochemical–hydrothermal route. The effect of aluminum substitution on the structural, physico-chemical and morphological characteristics are presented by comparison with non substituted materials. The lithium insertion properties of these materials are studied in relation with their structural characteristics.

2. Experimental

The syntheses were performed in a stainless steel autoclave equipped with outlets connecting the working (Au plate, of ca.

* Corresponding author. Tel.: +33 2 40 37 39 12; fax: +33 2 40 37 39 95.
E-mail address: dominique.guyomard@cnrs-imn.fr (D. Guyomard).

0378-7753/$ – see front matter © 2006 Elsevier B.V. All rights reserved.
doi:10.1016/j.jpowsour.2006.10.030

28 cm^2), counter (vitreous carbon plates, of ca. 28 cm^2) and Ag^+/Ag reference electrodes to a potentiostat (Mac Pile, Claix, France) used in galvanostatic mode with an oxidation current. The synthesis solution was prepared by dissolution of $MnSO_4$ (0.3 M) in distilled water. To probe the effect of Al^{3+} ions on the synthesis and on the obtained material, $Al_2(SO_4)_3$ (0.3 M) was added to the starting solution. A constant anodic current (I = 10 or 1000 mA) was applied to the synthesis solutions at a temperature of 92, 113 and 140 °C. To keep a good homogeneity in composition and structure, the synthesis was stopped when about 600 mg of material were obtained. After the synthesis, the solid was removed from the electrode, rinsed thoroughly with distilled water and dried for 2 h at 75 °C. The morphology of the materials was studied using a JEOL JSM 6400F scanning electron microscope (SEM) operating at 7 keV.

Before the lithium insertion studies, the materials were manually ground in a mortar for a few minutes and heated at 250 °C for 16 h to remove adsorbed water and decrease the amount of structural water. X-ray diffraction (XRD) patterns (Cu Kα radiation) were obtained using a Siemens D5000 Bragg-Brentano ($\theta-2\theta$ configuration) diffractometer for the 2θ range, 10–75°. For extensively twinned γ-MnO_2 compounds characterized by Mt ≥ 50%, the FWHM of the (1 1 0) line was determined by simulation of the diffraction patterns by using the program PROLIX. Chemical compositions were determined by atomic absorption spectroscopy with inductively coupled plasma (AAS/ICP analysis), by energy depressive X-ray analysis (EDS) in a scanning electron microscope. EDS analyses were performed at the nanocrystal scale using a CM30 transmission electron microscope (TEM) operating at 300 kV. Thermogravimetric analysis (TG) was used to determine the water content in our products. Measurements of specific surface area were carried out with the Brauner, Emmett and Teller (BET) method using a Micromeritics 2010 apparatus (with N_2 as adsorbing gas).

Studies of lithium insertion behavior were performed with standard two-electrodes Swagelok cells made of a composite positive electrode (70 wt.% active material, 20 wt.% carbon black, 10 wt.% PVDF binder), a separator soaked in the electrolyte of composition (1M $LiPF_6$ in 2:1 ethylene carbonate (EC): dimethyl carbonate (DMC)), and a lithium metal negative electrode. Batteries were cycled in potentiodynamic (20 mV h^{-1}) and galvanostatic modes using a MacPile system (Biologic, Claix, France) in the voltage range 2–4 V versus Li electrode.

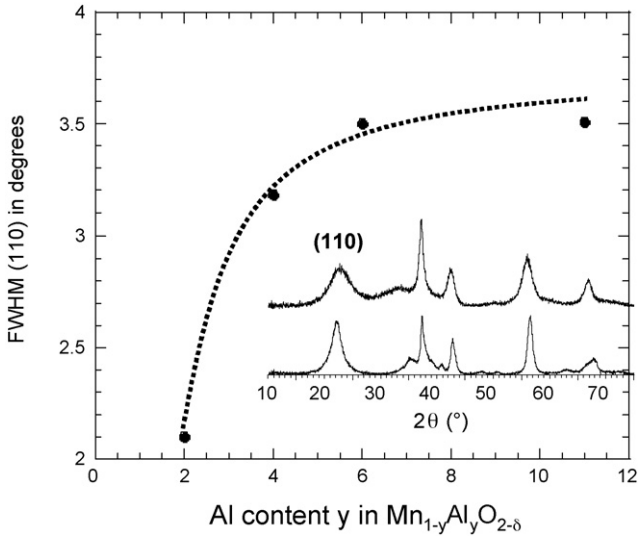

Fig. 1. Relationship between the broadening of the line (1 1 0) and the aluminum content in γ-$Mn_{1-y}Al_yO_{2-\delta}$. The corresponding XRD diffraction patterns for γ-$Mn_{0.89}Al_{0.11}O_{1.95}$ and $Mn_{0.97}Al_{0.03}O_{1.99}$ are given as well.

3. Results and discussion

3.1. Synthesis

A constant anodic current was applied between the working and the counter electrodes leading to the formation of brown MnO_2 compounds according to the following reaction:

$$Mn^{2+} + 2H_2O \Leftrightarrow MnO_2 + 4H^+ + 2e^-$$

In the presence of dissolved Al^{3+} cations, these cations are homogeneously incorporated into the MnO_2 structure, as shown by ICP measurements (see below).

3.2. X-ray diffraction

A variety of non substituted and Al-substituted MnO_2 materials have been synthesized by using the electrochemical–hydrothermal route. A systematic XRD study was undertaken to determine the average structure of the obtained materials. Single α-, β-, γ-MnO_2 phases and phase mixtures were obtained according to the experimental conditions [4].

XRD patterns of two γ-$Mn_{1-y}Al_yO_{2-\delta}$ compounds are shown in Fig. 1. Independently of the aluminum content, XRD patterns of these γ compounds exhibit only a few broad lines,

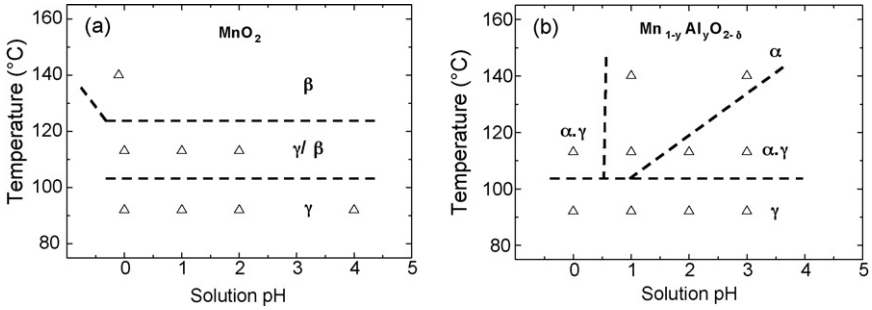

Fig. 2. Phase diagrams in the temperature-pH plane obtained by oxidative electrodeposition from (a) $MnSO_4$ solutions and (b) $MnSO_4/Al_2(SO_4)_3$ solutions. γ/β indicates a macroscopic mixture of the two phases and α·γ means a topotactic relationship between the two phases α and γ.

the lines (2 2 1) and (4 2 0) having completely merged, which is typical of highly disordered γ-MnO_2 materials [2]. The amount of microtwinning defects for these materials being superior or equal to 50%, the usual methods of characterization [2,3] do not lead to a structural classification. According to recent results [6], the broadening and the decrease in intensity of the (1 1 0) line can be related to an increase of the structural disorder. In our case, an increase in the aluminum content leads to a broadening of the (1 1 0) line (Fig. 1), thus indicating that the structural disorder increases with increasing aluminum content.

Fig. 2 shows phase diagrams as a function of pH and temperature, established from XRD patterns, for compounds synthesized from $MnSO_4$ (for comparison) and $MnSO_4/Al_2(SO_4)_3$ solutions. For non substituted compounds, at 92 °C, the γ-MnO_2 phase is formed. Increasing the temperature leads first to the formation of mixtures of γ- and β-MnO_2 phases and then to the formation of single β-MnO_2 phase. For compounds synthesized from $MnSO_4/Al_2(SO_4)_3$ solutions, the Al-containing γ phase is synthesized at 92 °C. Increasing the temperature induces first the formation of α·γ mixture and then the formation of α phase. α·γ means the existence of a topotactic orientation relationship between α- and ramsdellite-like phase [7]. The presence of aluminum in the compounds stabilizes the α phase at higher temperature (and thus higher pressure), which is unexpected because the α phase has the most open structure among MnO_2 materials synthesized in this study, with its 2 × 2 channels.

3.3. Physico-chemical characterizations

Systematic AAS/ICP and EDS analyses were carried out for compounds synthesized from $MnSO_4/Al_2(SO_4)_3$ solutions. It was shown that the aluminum content is homogeneous in the single γ and in the mixed α·γ phases. Fig. 3 illustrates the evolution of the aluminum content as a function of the solution pH in $Mn_{1-y}Al_yO_{2-\delta}$ powder. The Al/(Al + Mn) ratio increases with the solution pH. For γ-$Mn_{1-y}Al_yO_{2-\delta}$ compounds synthesized at 92 °C, the maximum aluminum content (of ca. 0.16) is reached for a solution pH equal to 3. An increase in temperature leads to an increase in the Al/(Al + Mn) ratio and to the formation of the mixed α·γ phases. Most of the analysis results were confirmed by EDS analysis at the nanocrystal scale in a TEM. Whatever the synthesis conditions were, the aluminum content was found

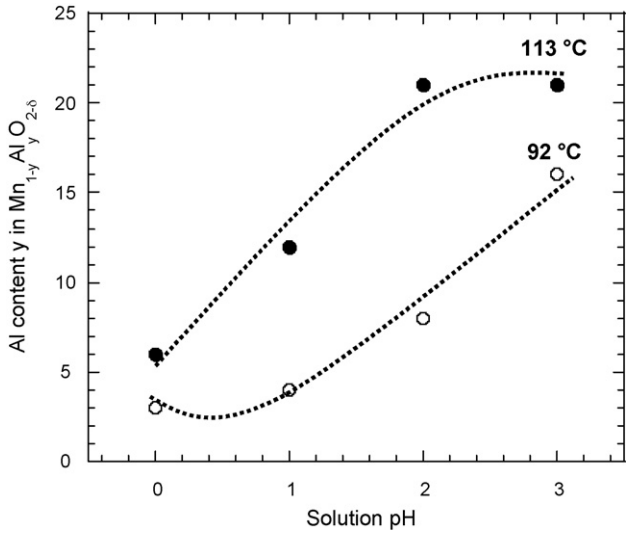

Fig. 3. Evolution of the aluminum content y (in percent) as a function of the solution pH in $Mn_{1-y}Al_yO_{2-\delta}$ at 92 °C (◯) and at 113 °C (●).

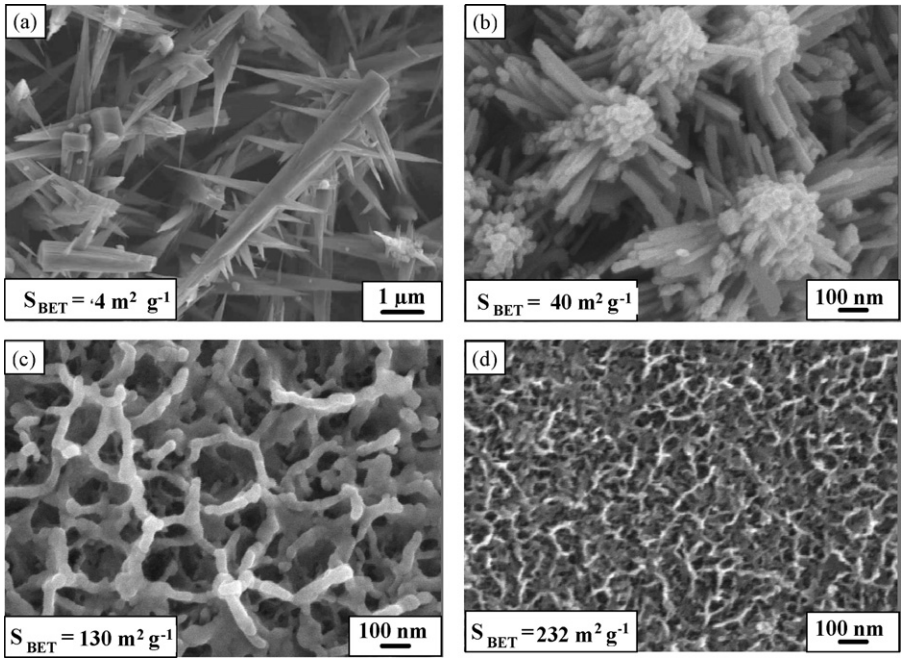

Fig. 4. SEM photographs of materials obtained at 92 °C with an applied current I = 10 mA. (a) non substituted γ-MnO_2 compound synthesized at pH 4, (b) and (c) Al-substituted γ-MnO_2 compounds synthesized at pH 0 and pH 3, respectively, and (d) Al-substituted γ-MnO_2 compound synthesized at pH 3 and with an applied current I = 1 A.

to be homogeneous throughout the sample in agreement with a substitution process.

TG/DSC analyses were performed on non substituted and Al-substituted MnO_2 materials to determine the total water content, n, in $MnO_2.nH_2O$. For non substituted γ-MnO_2 materials, the n value was found to range between 0.03 and 0.15, while this value was higher for Al-substituted MnO_2 materials (0.15–0.75). According to Poinsignon et al. [8], this increase can be attributed to an increase of the structural disorder in the materials as it was shown by XPS that the percentage of adsorbed water increases when the amount of microtwinning Mt increases.

3.4. Morphology

Fig. 4a and c show the surface morphology of the γ-MnO_2 (Fig. 4a) and γ-$Mn_{1-y}Al_yO_{2-\delta}$ (Fig. 4c) materials synthesized under the same conditions. The presence of aluminum in the structure leads to a sharp decrease in the particles size, and to a concomitant drastic increase in the surface area. As a matter of fact, the surface of the non substituted material (Fig. 4a) is made up of bundles of needles with a section ranging between 100 and 500 nm and the associated surface area is of ca. 4 $m^2\,g^{-1}$. The surface of the Al-substituted compound (Fig. 4c) consists of "nanowires" interconnected to each other with a section of ca. 50 nm, leading to a surface area of ca. 130 $m^2\,g^{-1}$.

Fig. 4b and c illustrate the effect of an increase in the solution pH, and thus in the aluminum content on the surface morphology of the materials. We can note that an increase in the solution pH, i.e. an increase in aluminum content, induces a change in surface morphology and a significant increase of the surface area. Increasing the current from 10 mA (Fig. 4c) to 1 A (Fig. 4d) leads to a decrease of the section of the "interconnected nanowires" and to an important increase of the surface area (from ∼130 to ∼232 $m^2\,g^{-1}$).

To conclude this part, it appears clearly that changes in the synthesis conditions (presence or not of Al^{3+}, pH) lead to drastic changes in the particle shape and size, which could be explained by changes in the nucleation-growth mechanism.

3.5. Lithium insertion study

Lithium insertion study has been performed on dehydrated samples. Fig. 5 shows the current versus voltage curves for a non substituted γ-MnO_2 material (for comparison) (Fig. 5a) and for a γ-$Mn_{1-y}Al_yO_{2-\delta}$ compound (Fig. 5b), measured at low rate. The two first cycles are different for each compound, marking an irreversible transformation during the first discharge, which is usual for the γ structure of manganese oxides. The width of the peaks associated to the electrochemical Li insertion phenomena is larger for the Al-substituted compound compared to the non substituted one. The Al-substituted compounds are heavily faulted. The larger peak width can be attributed to the higher structural disorder present (higher level of microtwinning Mt). It agrees with previous studies [9] indicating, that the amorphisation of a compound involves a broadening of the voltage range of the insertion processes.

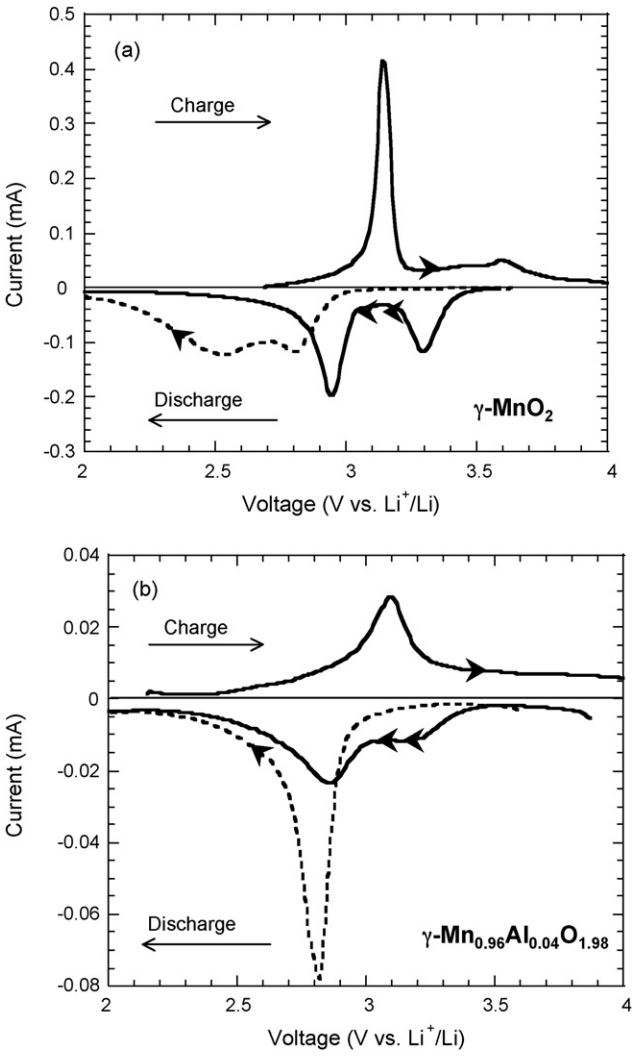

Fig. 5. Current vs. voltage curves at first discharge–charge cycle (dotted line) and second discharge cycle (solid line) measured in potentiodynamic mode (20 mV h^{-1}), for (a) a non substituted γ-MnO_2 material characterized by the structural parameters ($P_r = 40$, Mt = 20) and for (b) an Al-substituted γ-MnO_2 compound characterized by ($P_r = 39$, Mt ≥ 50).

Table 1
Reversible capacity Δx for non substituted and Al-substituted γ-MnO_2 compounds characterized by a high level of microtwinning (Mt ≥ 50%) obtained at the second discharge in cyclic voltammetry (20 mV h^{-1}) (noted Δx(2D)) and at the 20th discharge in galvanostatic discharge (C/10) (noted Δx(20D))

Mode	Intrinsic reversible capacity (C/100), Δx(2D)	Cycled reversible capacity (C/10), Δx(20D)
γ-MnO_2 (50, ≥50)	0.42	0.36
γ-$Mn_{0.96}Al_{0.04}O_{1.98}$ (39, ≥50)	0.49	0.38
γ-$Mn_{0.89}Al_{0.11}O_{1.95}$ (50, ≥50)	0.47	0.34

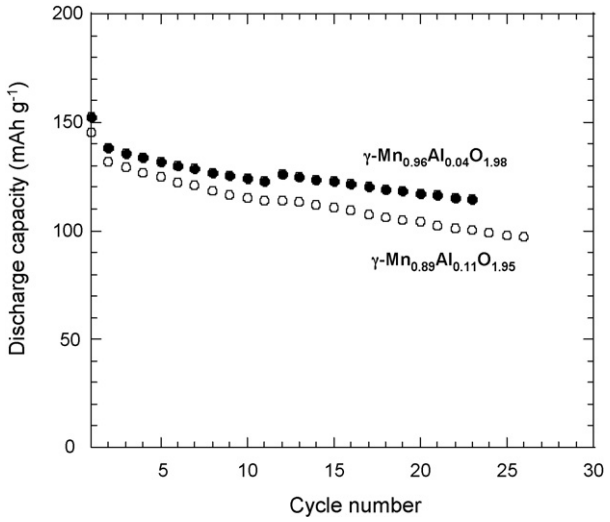

Fig. 6. Discharge capacity as a function of cycle's number for γ-$Mn_{0.96}Al_{0.04}O_{1.98}$ and γ-$Mn_{0.89}Al_{0.11}O_{1.95}$ compounds obtained in galvanostatic mode (*C*/10).

Knowing that the reversible Li insertion capacity strongly depends on the structural parameters (P_r, Mt) [4], we compare in Table 1 the reversible capacity of non substituted and Al-substituted γ-MnO_2 materials characterized by the same range of microtwinning content (corresponding to Mt ≥ 50%). For a cycling rate near thermodynamic equilibrium (i.e. *C*/100), the intrinsic reversible capacity is higher for γ-$Mn_{1-y}Al_yO_{2-\delta}$ compounds than for non substituted ones. But increasing the aluminum content leads to a slight decrease in the intrinsic reversible capacity. These limitations could be the consequence of the structural disorder induced by the increase of the aluminum content, as determined above.

At a faster rate of *C*/10, the reversible capacity decreases for all the compounds. The capacity fading is higher for γ-$Mn_{1-y}Al_yO_{2-\delta}$ compounds than for non substituted ones. No significant influence of the Al content on the fading rate was measured, as shown in Table 1 and as illustrated in Fig. 6 for the example of two Al contents. Given the smaller particle size of Al-substituted materials and their high surface area compared to non substituted ones, we deduce that the intrinsic kinetic limitations of Al-substituted materials are stronger than those of γ-MnO_2 compounds.

4. Conclusions

We have shown that the electrochemical–hydrothermal method can be used to synthesize Al-substituted MnO_2 materials having the α- and γ-structure types or mixtures of structure types. The γ-$Mn_{1-y}Al_yO_{2-\delta}$, nH_2O materials thus obtained are characterized by a high level of microtwinning (Mt ≥ 50%), and a very high surface area associated to a high total water content *n*. "Interconnected nanowires" were synthesized in one single step under some experimental conditions. The lithium insertion studies have shown that the presence of aluminum in the compounds allows to increase the intrinsic reversible Li insertion capacity. However, an increase in the aluminum content induced an increase of the structural disorder and a concomitant slight decrease in reversible capacity whatever the cycling rate.

Further studies are in progress to get a better understanding of the effect of the structural parameters in the γ-MnO_2 structure on the Li insertion properties.

References

[1] P.M. De Wolff, Acta Crystallogr. 12 (1959) 341.
[2] Y. Chabre, J. Pannetier, Prog. Solid State Chem. 23 (1995) 1.
[3] L.I. Hill, A. Verbaere, D. Guyomard, J. Power Sources 119–121 (2003) 226.
[4] L.I. Hill, A. Verbaere, D. Guyomard, J. Electrochem. Soc. 150 (2003) D135.
[5] S. Bodoardo, N. Penazzi, P. Spinelli, M. Arrabito, J. Power Sources 94 (2001) 194.
[6] L.I. Hill, A. Verbaere, J. Solid State Chem. 177 (2004) 4706.
[7] L.I. Hill, R. Portal, A. Verbaere, D. Guyomard, Electrochem. Solid-State Lett. 4 (2001) A180.
[8] C. Poinsignon, G. Berthomé, B. Prélot, F. Thomas, F. Villiéras, J. Electrochem. Soc. 151 (2004) A1611.
[9] S. Jouanneau, S. Sarciaux, A. Le Gal La Salle, D. Guyomard, Solid State Ionics 140 (2001) 223.